An investigation of the damage mechanisms and fatigue life diagrams of flax fiber-reinforced polymer laminates

Ihab El Sawi · Zouheir Fawaz · Redouane Zitoune · Habiba Bougherara

Abstract In this paper we investigated the fatigue damage of a unidirectional flax-reinforced epoxy composite using infrared (IR) thermography. Two configurations of flax/epoxy composites layup were studied namely, $[0]_{16}$ unidirectional ply orientation and $[\pm 45]_{16}$. The high cycle fatigue strength was determined using a thermographic criterion developed in a previous study. The fatigue limit obtained by the thermographic criterion was confirmed by the results obtained through conventional experimental methods (i.e., Stress level versus Number of cycles to failure). Furthermore, a model for predicting the fatigue life using the IR thermography was evaluated. The model was found to have a good predictive value for the fatigue life. In order to investigate the mechanism of damage initiation in flax/epoxy composites and the damage evolution, during each fatigue test we monitored the crack propagation for a stress level and at different damage stages, a direct correlation between the percentage of cracks and the mean strain was observed.

I. El Sawi · H. Bougherara (✉)
Department of Mechanical and Industrial Engineering, Ryerson University, Toronto, ON, Canada
e-mail: habiba.bougherara@ryerson.ca

Z. Fawaz
Department of Aerospace Engineering, Ryerson University, Toronto, ON, Canada

R. Zitoune
Institut Clément Ader (INSA, UPS, Mines Albi, ISAE), Université de Toulouse, Toulouse, France

Introduction

Polymer materials reinforced with plant-based fibers such as flax, hemp, jute, and sisal have been considered by numerous studies as potential alternative materials to glass fiber-reinforced plastics (GFRP) [1–4]. Like GFRP, natural fiber-based composites are inherently more susceptible to variations in manufacturing processes. Besides, in structural applications, such materials are often subjected to cyclic loads which cause progressive damage and may lead to long-term failure of the structure. Therefore, the knowledge of the fatigue behavior including damage mechanisms and stress level versus number of cycles to failure, often referred to as S–N curve, is required for designing composite structures and predicting their fatigue life.

Most engineering materials exhibit a safe stress level below which failure is not considered to occur. This safe stress is called the endurance limit or the fatigue limit. For metallic materials this stress level can be clearly defined. However, fiber-reinforced polymer matrix composites (PMC) do not typically have a fatigue limit. Instead, they undergo progressive damage such as matrix cracking, delamination, interface fiber/matrix failure, fiber breakage, etc. This damage accumulation process takes place during the entire life of the material and eventually leads to failure even at low applied stresses [5, 6], hence the concept of high cycle fatigue strength (HCFS) is opposed to fatigue limit. Conventional methods for evaluating the fatigue limit or HCFS are very expernsive as the case may necessitate the use of a large number of samples. As a consequence of recent progress in the development of high-resolution infrared detectors for infrared (IR) thermographic cameras the application of theoretical concepts of thermoelasticity has been made possible [7–10]. Thermoelastic stress

measurements are based on small temperature variations of the order of 0.001 °C that occur when a material is subject to a change in elastic strain. The IR thermography technique has been proven to be a reliable nondestructive and non-intrusive technique for the rapid evaluation of fatigue damage and fatigue limit of metallic materials [11–18].

For composite materials, the IR thermography technique has been extensively used as a tool for qualitative monitoring of damage evolution. For instance, Quaresimin et al. [19] used the IR thermography to study the notch sensitivity of various GFRP specimens. In another study, Dattoma et al. [20] used the IR thermography for detecting the glue infiltration, water ingress, and disbonds on a blade of a wind turbine made of composite materials. In contrast, only few studies have been reported in the literature focusing on a temperature rise method for rapid evaluation of fatigue limit of fiber-reinforced composite materials. Montesano et al. [21] have successfully applied the IR techniques for the identification of the fatigue limit of a braided carbon fiber polyimide composite. Kamara [22] has also studied the damage evolution and determined the fatigue limit of a woven carbon fiber-reinforced polymer material using IR thermography technique.

In contrast to the abundance of studies dealing with the fatigue behavior of carbon and glass fiber-reinforced polymers, the fatigue behavior of natural fiber (plant-based)-reinforced polymers is less well understood with very limited information being currently available in the literature [3, 23–29]. This fact has been pointed out in a very recent research article by Shah et al. [30]. When narrowing down our research to the flax fibers, only one research work is found to deal with the fatigue behavior and endurance of this type of plant fiber [31] and no work has investigated the application of IR thermography for the determination of the fatigue limit of natural fibers-reinforced polymer composites.

The aim of this study is, therefore, to investigate the fatigue performance of flax fiber-reinforced composites. In particular, the study explores the use of IR thermography techniques for the in situ characterization of damage and, consequently, fatigue life prediction of flax fiber-reinforced composites during mechanical fatigue testing.

Experimental methods

Composite material

Flax/epoxy prepreg was purchased from LINEO, Belgium. The product type is a unidirectional (UD) flax fiber treated by a patented sizing and drying process (US Patent No. 8080288) and impregnated with a partially cured epoxy resin system (Huntsman LY5150). The flax/epoxy prepreg has an area density of 180 g/m^2 with an epoxy content of 50 % per weight. Flax/epoxy laminate plates were manufactured using 16 layers of 300 mm X 300 mm sheets with a $[0]_{16}$ unidirectional ply orientation and $[\pm45]_{16}$. The material was placed on a plate in a sealed vacuum bagging set-up and cured in an autoclave at 150 °C for 2 h under 4-bar pressure while a 0.7-bar vacuum was maintained during the entire cure cycle.

Testing procedures

The tested specimens were individually cut from the laminate plates in rectangular beams using a diamond wheel. All specimens had 25 mm width, 250 mm length, and 3 mm thickness. Four samples were tested for each type of test.

The static tensile tests and tension–tension fatigue tests were conducted on a servo-hydraulic MTS test machine equipped with a 100 kN load cell capacity. Strain measurements were obtained using an extensometer with a 25 mm gage length, placed at the center of all specimens. The static tests were performed in accordance with ASTM standard D3039 [32], at a displacement rate of 2 mm/min. The ultimate tensile strength (UTS), ultimate strain, and modulus of the composite were accordingly determined. Fatigue experiments were conducted in accordance with the ASTM standard D3479 [33] at room temperature and under load control with a minimum to maximum stress ratio of 0.1 and a cyclic frequency of 5 Hz. The samples were mounted in the grips using a 40 lb.in torque. The temperature rise versus applied cyclic load curves were obtained from stepwise cyclic load increment tests whereby the cyclic load was kept constant for a specific number of cycles, namely 7000 cycles, in order to reach the steady temperature. Starting from the lowest cyclic load levels, loading was incremented stepwise, 7000 cycles at each step, and so forth until failure of the sample occurred. The overall rise in specimen's temperature was recorded for each cyclic load level at the end of each 7000 cycles run. Those tests were followed by conventional fatigue tests in order to determine the composite's S–N curve. Fatigue limit was assumed to be reached for all tests that did not produce fatigue failure after 6 million cycles.

IR measurement

The IR camera used in this study is a FLIR SC5000 Series. The camera's resolution is 320×240 pixels with a temperature sensitivity of 20 mK for accurately monitoring the temperature variation. The IR camera was synchronized to the mechanical test controller in order to trigger the acquisition of images at the maximum stress loading in each loading cycle and avoid temperature fluctuation due to any possible reversible thermoelastic heating.

Scanning electron microscope

Pre-failure and post-failure microscopic observations of the cross section of a number of fatigue-tested specimens were performed to inspect the microstructure and the damage progress in the flax/epoxy composites. The observations were done using a scanning electron microscope SEM (JEOL JSM-6380, Tokyo, Japan). The closest applicable standard used for the samples preparation technique was the ASTM E2015–04 "Standard Guide for Preparation of Plastics and Polymeric Specimens for Microstructural Examination."

The samples were sectioned in random locations in the gage area and close to the gage area. Four small samples for microscopic observation were cut out of each sample fatigue-tested specimen. A fine cut was made using an ultra-thin diamond blade (0.35 mm thick)—SMART CUT^{TM}—from UKAM Industrial Superhead Tools, Valencia, CA, USA. Then, each specimen was embedded in an epoxy resin and was left to cure at room temperature. The cutting process results in mechanical deformation and artefacts below the sample surface. These artefacts were removed by subsequent grinding and polishing steps. The first grinding steps were performed using successive silicon carbide abrasive paper size in the following order P320-P600-P1200; this first step took approximately 30 min in order to remove the maximum of artefacts. Finally, polishing steps were performed during 15 min using a fine diamond abrasive (6 μm then 1 μm particle size) on soft plane cloths. The grinding procedure resulted in the removal of the surface below the cut location. Approximately 10 mm of material was removed after the grinding/polishing process. The authors estimated that the artifacts induced by the cutting are removed and the observed micrographs represent the actual microstructure of the specimen.

Results and discussion

Determination of the S–N curve and the HCFS using conventional method

At first, quasi-static tests were performed in order to determine the ultimate tensile strength (UTS) of the specimens. The stress versus strain plots for the studied composites are shown in Fig. 1. The maximum stress amplitude to be applied for each fatigue test is defined as a percentage of the average value of the UTS. The Quasi-static tests revealed an average UTS value of the $[0]_{16}$ and $[\pm45]_{4S}$ laminates of 304 and 68.4 MPa, respectively. A minimum of three test specimens were used for each applied maximum stress and the range of maximum stresses applied was
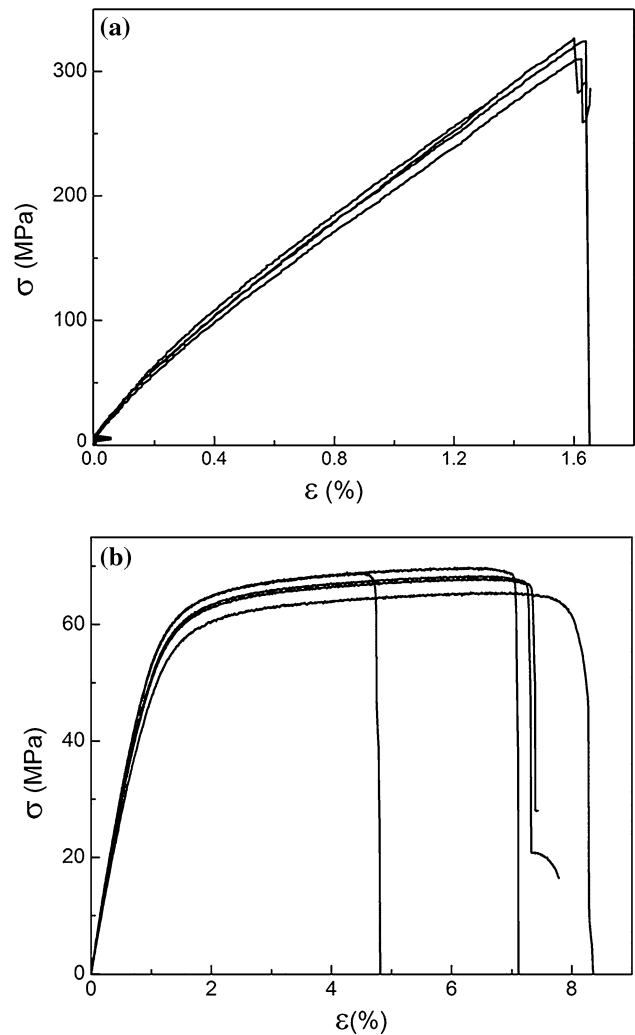

Fig. 1 Stress versus strain plots for all the samples tested under quasi-static tensile tests; a $[0]_{16}$ flax/epoxy laminates and b $[\pm45]_{4S}$ flax/epoxy laminates

from 40 to 80 % of the UTS. The results of the fatigue tests (S–N curves) at different stress levels are presented in Figs. 2 and 3. The data with arrowhead at 6 million cycles indicate that the specimens did not fail at the corresponding stress level. The HCFS is found to be in the range of 45 to 50 % of the UTS for the $[0]_{16}$ laminates and in the range of 55 to 60 % for the $[\pm45]_{4S}$ laminates. Both composite laminates exhibit a linear profile when the S–N curves are plotted in a semi-log scale.

Fatigue damage analysis

In order to investigate the formation and propagation of microdamage in the studied composite laminates we carried out interrupted fatigue tests at 70 % of the UTS, where the average number of cycles to failure (N_f) is 83625 cycles and 91874 cycles for the $[0]_{16}$ laminates and $[\pm45]_{4S}$
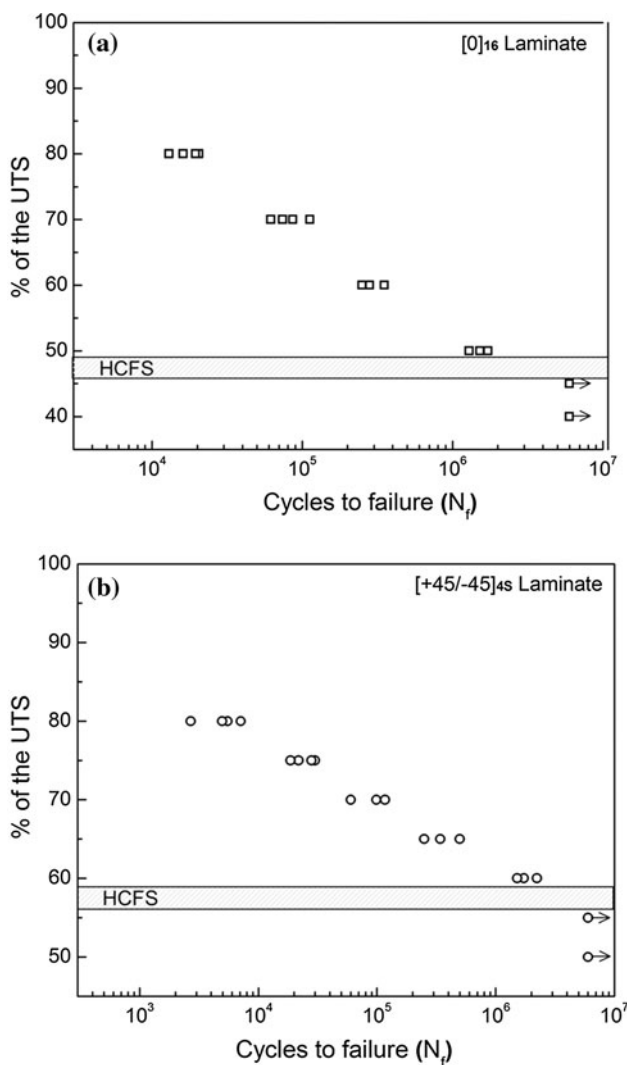
Fig. 2 S–N curve (**a**) for the $[0]_{16}$ flax/epoxy laminates (**b**) for the $[\pm45]_{4S}$ flax/epoxy laminates ($R = 0.1$, $f = 5$ Hz, UTS = 304 MPa)

laminates, respectively. We conducted three fatigue tests, each on two specimens. The first two specimens were tested until 1/3 of N_f; then the test was interrupted and the two other specimens were tested until 2/3 of N_f and finally two specimens were tested until failure. The specimens were then sectioned at different locations and were prepared for SEM observations. SEM micrographic analysis after different fatigue damage levels revealed that the flax/epoxy composites undergo different damage mechanisms depending on the layup and ply orientation. Three main fatigue microdamage mechanisms can be distinguished in the case of the $[0]_{16}$ laminate as can be seen in Fig. 3a, b and c. The damage types (microcracks) are labeled in the figures with numbers. Label 1 represents a section of a bundle of flax fibers (50–100 fibers) bonded together by pectin. Individual flax fibers contain holes in the middle (lumen); yet from the examination of the micrographs at

higher magnifications, it appears that the cracks do not propagate from these holes. Label 2 shows that the cracks nucleate inside the bundles between fibers, which means that the cracks initiate when the pectin fails causing delamination between adjacent fibers. At 2/3 of N_f (Fig. 3b) the cracks continue to grow slightly and propagate inside the bundle (from one end to the other) without further propagating in the matrix rich area (label 3). We were also able to distinguish an interface bundle–matrix failure at this stage of the fatigue damage as represented by Label 4. At the total failure of the laminate the microcracks appear to have further grown in the bundles with subsequent propagation in the matrix (Label 5) and the number of cracks (or density of crack) is considerable. The bundle–matrix interface did not fail after the total failure of the $[0]_{16}$ laminates. We can assume that the failure happens after the mechanical degradation of the cellulosic fibers with the increasing number of fatigue cycles.

Similarly, in the case of the $[\pm45]_{4S}$ laminates represented in Fig. 3d, e and f the damage occurs in the same manner as in the $[0]_{16}$ laminates, that is, pectin failure and cracks inside a bundle. Label 6 represents a cross section of a flax fibers bundle in $45°$. At an advanced stage of the damage, 2/3 of N_f, the interface bundle–matrix starts to fail (Label 7) and finally the cracks propagate in the resin and interconnect with each other passing through the matrix-rich zone (Label 8). The percentages of cracks are calculated using ImageJ Software from National Institute of Health. The results are reported in Table 1.

The dynamic modulus E* was determined for each laminate and for different applied stress levels by calculating the slope of the linear part of the strain versus stress curve at each cycle. The dynamic modulus for the $[0]_{16}$ and $[\pm45]_{4S}$ laminates are plotted against the normalized number of cycle (Cycle N/total cycles to failure N_f) and presented in Figs. 4a and 5a, respectively. In the case of $[0]_{16}$ laminates, E* is found to increase with number of cycles until reaching a specific value prior to failure: E* = 32.5 GPa. An average increase of the stiffness by 8 % is calculated. Similar hardening behavior was reported by Liang et al. [31] for flax/epoxy composite laminates $[0/90]_{3S}$. Plant-based fibers are known to have such hardening behavior. For instance, Baley [34], Spatz et al. [35], and Silva et al. [26] have observed the increase of the stiffness of single plant-based fibers (Sisal fibers and flax fibers) when investigating their behavior under cyclic loading. This phenomenon was attributed by the authors to the progressive reorientation of the cellulose microfibrils toward the loading direction.

The mean strain is determined from the maximum and minimum strains and presented in Figs. 4b and 5b for the $[0]_{16}$ and $[\pm45]_{4S}$ laminates, respectively. For both laminates the strain increases rapidly in the early part of the
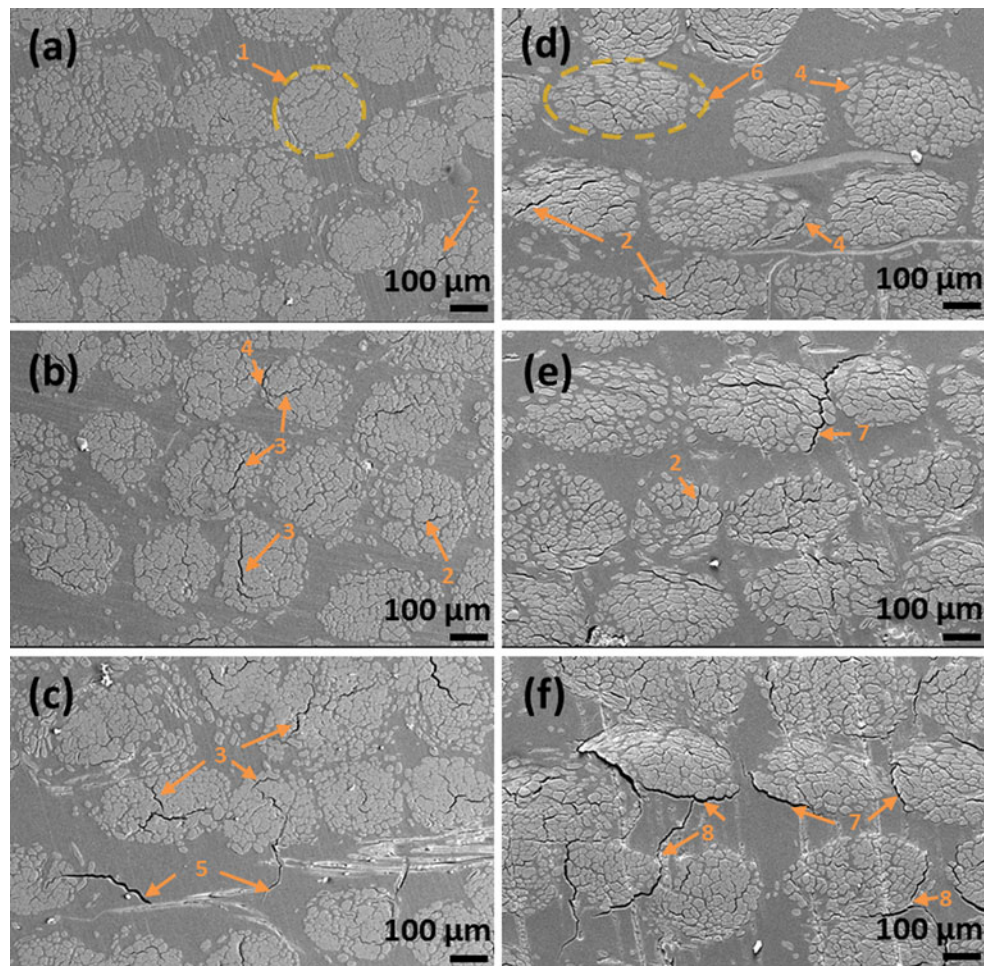
Fig. 3 SEM micrograph of the cross section of surface of the composites showing formation of microcracks at 70 % of the UTS and for different damage levels of the $[0]_{16}$ flax/epoxy laminates after 1/3 of N_f (**a**), 2/3 of N_f (**b**), and N_f (**c**); and the $[\pm45]_{4S}$ flax/epoxy laminates after 1/3 of N_f (**d**), 2/3 of N_f (**e**), and N_f (**f**)

Table 1 Crack density calculated using image analysis software at different levels of damage for 70 % of UTS stress level

N/N_f	% of Crack $[0]_{16}$ laminate	% of Crack $[\pm45]_{4S}$ laminate
0	0	0
1/3	0.495 (±0.033)	1.028 (±0.038)
2/3	0.510 (±0.025)	1.771 (±0.027)
1	0.635 (±0.024)	2.825 (±0.046)

test, then for the $[0]_{16}$ laminates a quasi-steady strain evolution is observed until the failure of the laminate. This steady strain was correlated with the SEM observations which reveal a very small increase of crack percentage in the $[0]_{16}$ during this cycling phase until failure, suggesting a sudden failure of the cellulosic fibers. Conversely, for the $[\pm45]_{4S}$ laminates, the second phase of fatigue cycling is described by an increase of the strain by a constant slope followed by an acceleration stage and the failure. The

analysis of the SEM images shows a very good concordance between the evolution of the cracks and the increase of the strain; see Fig. 5b.
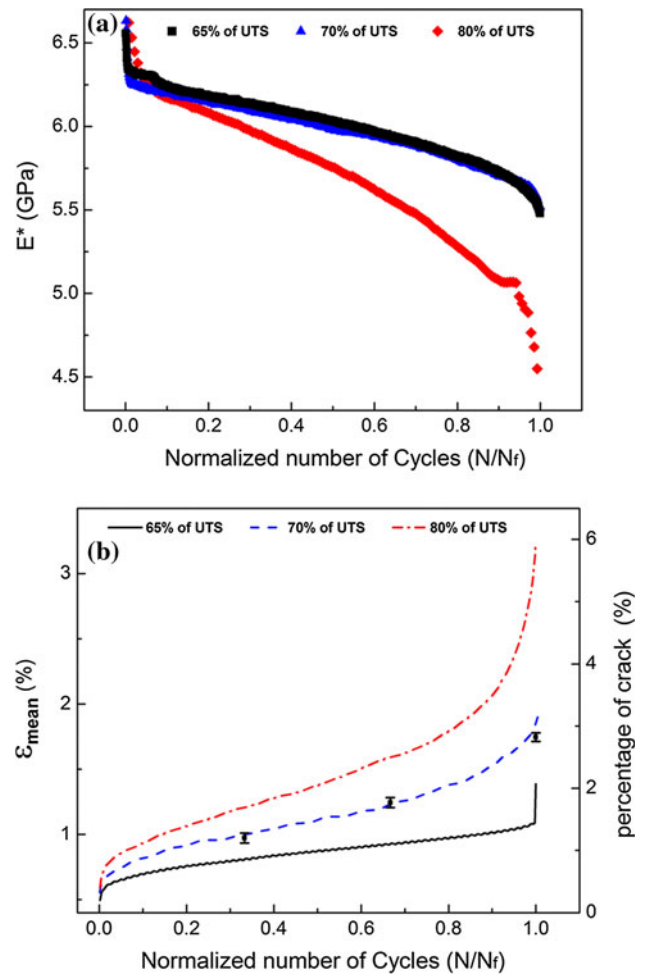
Determination of the S–N curve and the HCFS using IR thermography

Using the aforementioned IR camera we recorded the temperature increase of the flax/epoxy composite laminates during stepwise loading fatigue tests. The thermograms presented in Fig. 6a and b present the temperature increase as a function of the number of cycles for different loading levels for the $[0]_{16}$ and $[\pm45]_{4S}$ laminates, respectively. It is clear from the plots that after 4000 cycles the temperature rise levels off and reaches a constant temperature. During all the tests the recorded temperature was uniform across all the surface of the specimen until a certain level of stress, namely 65 % of the UTS in the $[0]_{16}$ laminates and 55 % of the UTS in the $[\pm45]_{4S}$ laminates. Above
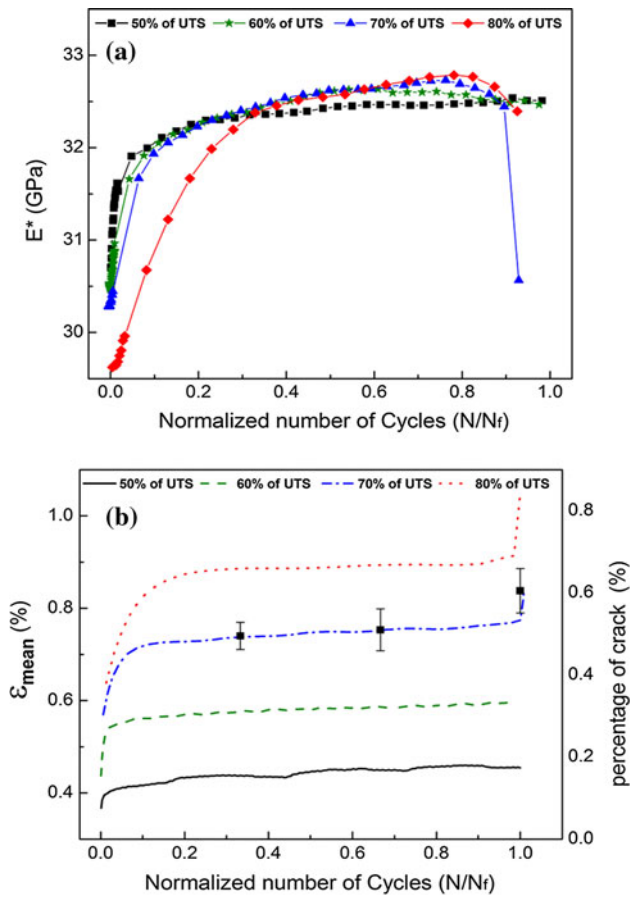
Fig. 4 **a** Typical dynamic elastic modulus E* versus normalized number of cycle (N/N_f) and **b** The *lines* represent the mean strain versus normalized number of cycle (N/N_f) and the *square symbols* with *error bars* represent the cracks percentage in the composite; $[0]_{16}$ flax/epoxy laminates

Fig. 5 **a** Typical dynamic elastic modulus E* versus normalized number of cycle (N/N_f) and **b** The *lines* represent the mean strain versus normalized number of cycle (N/N_f) and the *square symbols* with *error bars* represent the cracks percentage in the composite; $[\pm45]_{4S}$ flax/epoxy laminates

these stress levels a temperature gradient appears on the surface of the sample with the hottest zone in the area where the failure happened later because of the stress concentration in that area. The failure happened at 80 and 85 % of the UTS for the $[0]_{16}$ and $[\pm45]_{4S}$ laminates, respectively. We noticed that prior to failure the temperature profile of the $[0]_{16}$ laminates reached a steady temperature whereas for the $[\pm45]_{4S}$ laminates the temperature kept on increasing until the total failure of the composite as shown in Fig. 6. The plots of the temperature versus the applied stress level (in % of UTS) are presented in Fig. 7. The bilinear nature of the data can be well seen from these graphs. We used a linear regression for each part of the plots and determined the HCFS which according to this technique corresponds to the intersection of the tow linear parts of the plot. The HCFS determined by the IR thermography method was 45.6 % of the UTS for the $[0]_{16}$ composite laminates and 57 % of the UTS for $[\pm45]_{4S}$ laminates. These values compare well with the HCFS found by the conventional methods.

In addition to the HCFS, IR Thermography can provide information to build up the S–N curve of the studied composite laminates. The procedure to determine the fatigue S–N curve using the IR technique is described in the work of Fargione et al. [17]. The author's hypothesis permits to establish a direct correlation between the temperature increase during a certain stress level and the number of cycles to failure at the same level of stress as shown in equation (1):

$$\Phi = \Delta T_i \cdot N_{fi} \tag{1}$$

Where N_{fi} is the total number of cycle at stress level σ_i, and ΔT_i is the temperature difference between the room temperature and the stabilized temperature at that stress level. The parameter Φ is a constant that is directly proportional to heat dissipation of the material and was defined by the authors to be the integral of the function $\Delta T = f(N)$ extended over the entire number of cycles N_f.
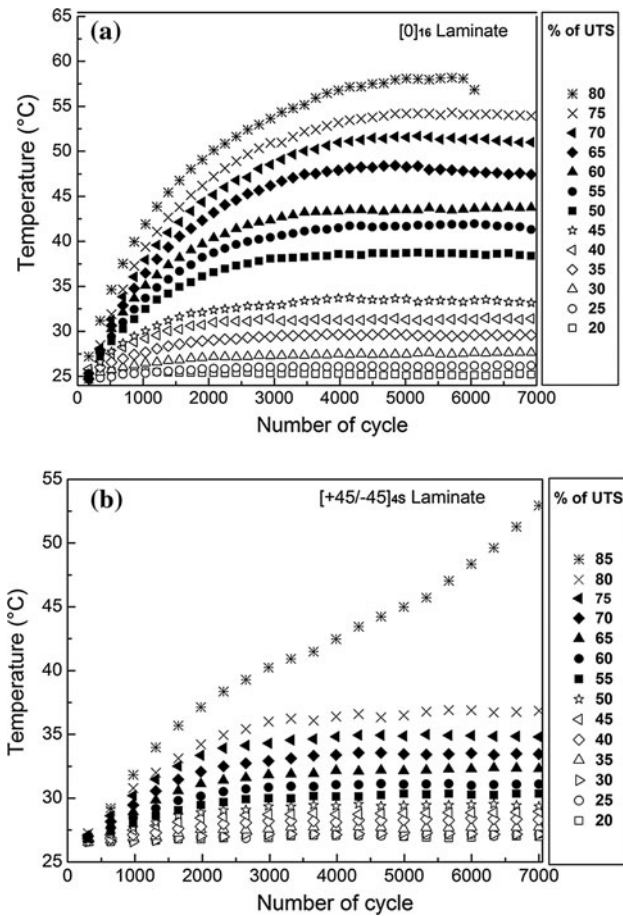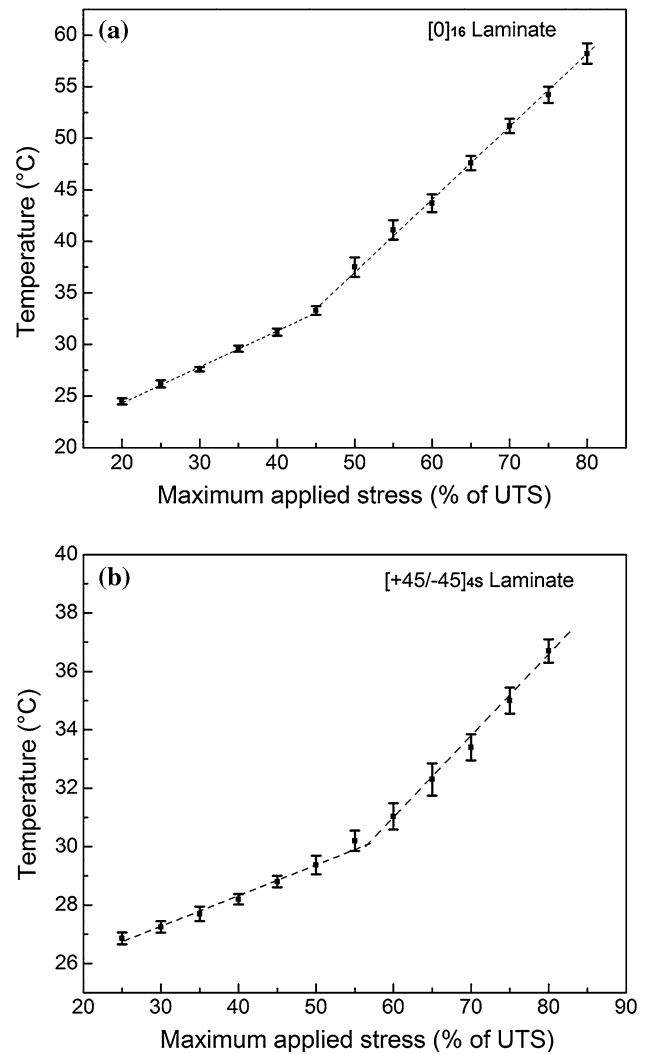
Fig. 6 Thermal variation versus number of cycle for maximum applied stress (**a**) for the $[0]_{16}$ flax/epoxy laminates and (**b**) for the $[\pm45]_{4S}$ flax/epoxy laminates

The above expression (Equation (1)) was initially developed for metallic materials. Montesano et al. [21] found that the integration function Φ is only a constant when multiplying the thermal change by the logarithm of the number of cycles. They have consequently modified Equation (1) to fit their thermal and fatigue experimental data on carbon fiber-reinforced polyimide composite. The modified equation is written as follows.

$$\Phi = \Delta T_i \cdot \mathrm{Log}(N_{\mathrm{fi}}) \tag{2}$$

The current thermal change data (ΔT) and fatigue data (N_{f}) for each corresponding stress level are used to calculate the integration parameter Φ using equation (2). The results for the $[0]_{16}$ and the $[\pm45]_{4S}$ laminates are presented in Table 2. The calculated Φ can be considered to be constant for each laminate. The average value of Φ ($\pm$standard deviation) was approximately $\overline{\Phi} = 118\ ^\circ\mathrm{C}$ (±19) for the $[0]_{16}$ laminate and $\overline{\Phi} = 35\ ^\circ\mathrm{C}$ (±2) for the $[\pm45]_{4S}$ laminate. The parameter was found to be constant regardless of the applied maximum stress. This means that by knowing only one stress value and the corresponding

Fig. 7 Average stabilized temperature versus the maximum applied stress (**a**) for the $[0]_{16}$ flax/epoxy laminates and (**b**) for the $[\pm45]_{4S}$ flax/epoxy laminates

Table 2 Integration parameter Φ for the $[0]_{16}$ laminates and for the $[\pm45]_{4S}$ laminates determined using equation (2)

% of the UTS	$[0]_{16}$ laminates			$[\pm45]_{4S}$ laminates		
	Log (N_{f})	ΔT (°C)	Φ (°C)	Log (N_{f})	ΔT (°C)	Φ (°C)
80	4.03754	33.5	135.3	3.70417	10.2	37.8
75	–	–	–	4.39110	8.5	37.3
70	4.92234	26.7	131.4	4.96319	6.9	34.4
65	–	–	–	5.56023	5.8	34.2
60	5.76815	19.6	113.7	–	–	–
50	6.87894	13.5	92.8	–	–	–

thermal increase one can define the integration constant Φ and subsequently determine the S–N curve of the studied material using equation (2) in the case of fiber-reinforced polymer materials.

Conclusions

In this work we demonstrated that IR thermography can be a useful technique for designing composite structures made of flax/epoxy materials and predicting their fatigue life. The experimental data from the IR thermography tests and the fatigue tests showed a good repeatability and low scattering. The high cycle fatigue strength estimated using an IR thermography-based technique was in very good accordance with the HCFS obtained using conventional methods. The use of this technique will result in more efficient use of composite of materials.

The damage initiation in flax/epoxy laminates seem to occur inside the fiber bundles between fiber–fiber interfaces suggesting that the bonding agent (pectin) is the weakest component in the flax/epoxy composite. As a result, during a cyclic loading, cracks will initiate and propagate through the interface between the elementary fibers within the bundles.

References

1. Wambua P, Ivens J, Verpoest I (2003) Natural Fibres: Can They Replace Glass in Fibre Reinforced Plastics? Compos Sci Technol 63:1259–1264. doi:10.1016/S0266-3538(03)00096-4
2. Fowler PA, Hughes JM, Elias RM (2006) Biocomposites: technology, environmental credentials and market forces. J Sci Food Agric 86:1781–1789. doi:10.1002/jsfa.2558
3. Katogi H, Shimamura Y, Tohgo K, Fujii T (2012) Fatigue behavior of unidirectional jute spun yarn reinforced pla. Adv Compos Mater 21:1–10. doi:10.1163/156855111x610226
4. Hughes M, Carpenter J, Hill C (2007) Deformation and fracture behaviour of flax fibre reinforced thermosetting polymer matrix composites. J Mater Sci 42:2499–2511. doi:10.1007/s10853-006-1027-2
5. Harris B (2003) Fatigue in composites: science and technology of the fatigue response of fibre-reinforced plastics. Woodhead Publishing Limited, Oxford
6. Vassilopoulos AP (2010) Fatigue Life Prediction of Composites and Composite Structures. Woodhead Publishing Limited, Oxford
7. Pitarresi G, Patterson E (2003) A review of the general theory of thermoelastic stress analysis. J Strain Anal Eng Des 38:405–417
8. Kelvin WTB (1878) On the thermoelastic, thermomagnetic, and pyroelectric properties of matter. Philos Mag 5:4–27
9. Greene R, Patterson E, Rowlands R (2008) In: Sharpe WN Jr (ed) Springer handbook of experimental solid mechanics. Springer, New York
10. Dulieu-Barton JM (1999) Introduction to thermoelastic stress analysis. Strain 35:35–39. doi:10.1111/j.1475-1305.1999.tb01123.x
11. Luong MP (1998) Fatigue limit evaluation of metals using an infrared thermographic technique. Mech Mater 28:155–163. doi:10.1016/S0167-6636(97)00047-1
12. Luong MP (1995) Infrared thermographic scanning of fatigue in metals. Nucl Eng Des 158:363–376. doi:10.1016/0029-5493(95)01043-H
13. Luong MP (1992) In: Jan E (ed) Thermosense XIVSPIE–the international society for optical engineering. Florida, Orlando
14. GA Kurilenko (2004) Science and Technology, 2004. KORUS 2004. Proceedingsof the 8th Russian-Korean International Symposium on, Vol. 3. p 32–34
15. JC Krapez, D Pacou, C Bertin, FOndéedr aérospatiales (2000) Application of lock-in thermography to rapid evaluation of fatigue limit in metals. Office national d″ etudes et de recherches a′ erospatiales
16. La Rosa G, Risitano A (2000) Thermographic methodology for rapid determination of the fatigue limit of materials and mechanical components. Intern J Fatigue 22:65–73. doi:10.1016/S0142-1123(99)00088-2
17. Fargione G, Geraci A, La Rosa G, Risitano A (2002) Rapid determination of the fatigue curve by the thermographic method. Intern J Fatigue 24:11–19. doi:10.1016/S0142-1123(01)00107-4
18. J-C Krapez, D Pacou (2002) Thermography detection of damage initiation during fatigue tests. Thermosense 435–449. doi:10.1117/12.459593
19. Quaresimin M, Guglielmino E (2000) In: Paolo P (ed) Proceedings of the fifth seminar on experimental techniques and design in composite materials. Trans tech publications, Cagliari
20. Dattoma V, Marcuccio R, Pappalettere C, Smith GM (2001) Thermographic investigation of sandwich structure made of composite material. NDT E Intern 34:515–520. doi:10.1016/S0963-8695(00)00082-7
21. Montesano J, Fawaz Z, Bougherara H (2013) Use of infrared thermography to investigate the fatigue behavior of a carbon fiber reinforced polymer composite. Compos Struct 97:76–83. doi:10.1016/j.compstruct.2012.09.046
22. Karama M (2011) Determination of the fatigue limit of a carbon/epoxy composite using thermographic analysis. Struct Control Health Monit 18:781–789. doi:10.1002/stc.485
23. Belmares H, Barrera A, Monjaras M (1983) New composite-materials from natural hard fibers. 2. Fatigue studies and a novel fatigue degradation model. Ind Eng Chem Prod Res Develop 22:643–652. doi:10.1021/i300012a024
24. Gassan J (2002) A study of fibre and interface parameters affecting the fatigue behaviour of natural fibre composites. Compos Part A 33:369–374. doi:10.1016/S1359-835X(01)00116-6
25. Towo AN, Ansell MP (2008) Fatigue evaluation and dynamic mechanical thermal analysis of sisal fibre-thermosetting resin composites. Compos Sci Technol 68:925–932. doi:10.1016/j.compscitech.2007.08.022
26. Silva FD, Chawla N, de Toledo RD (2009) An experimental investigation of the fatigue behavior of sisal fibers. Mater Sci Eng a-Struct Mater Prop Microstruct Process 516:90–95. doi:10.1016/j.msea.2009.03.026
27. Belaadi A, Bezazi A, Bourchak M, Scarpa F (2013) Tensile static and fatigue behaviour of sisal fibres. Mater Des 46:76–83. doi:10.1016/j.matdes.2012.09.048
28. Gassan J, Bledzki AK (1999) Possibilities for improving the mechanical properties of jute/epoxy composites by alkali treatment of fibres. Compos Sci Technol 59:1303–1309. doi:10.1016/S0266-3538(98)00169-9
29. Towo AN, Ansell MP (2008) Fatigue of sisal fibre reinforced composites: constant-life diagrams and hysteresis loop capture. Compos Sci Technol 68:915–924. doi:10.1016/j.compscitech.2007.08.021
30. Shah DU, Schubel PJ, Clifford MJ, Licence P (2013) Fatigue life evaluation of aligned plant fibre composites through S–N curves and constant-life diagrams. Compos Sci Technol 74:139–149. doi:10.1016/j.compscitech.2012.10.015
31. Liang S, Gning PB, Guillaumat L (2012) A Comparative Study of Fatigue Behaviour of Flax/Epoxy and Glass/Epoxy Composites. Compos Sci Technol 72:535–543. doi:10.1016/j.compscitech.2012.01.011
32. Astm Standard D3039/D3039 m-08 (2007) Standard test method for tensile properties of polymer matrix composite materials. Am Soc Test Mater

33. Astm Standard D 3479/D 3479 m-12 (2007), Standard test method for tension–tension fatigue of polymer matrix composite materials. Am Soc Test Mater

34. Baley C (2002) Analysis of the flax fibres tensile behaviour and analysis of the tensile stiffness increase. Compos Part A 33:939–948. doi:10.1016/S1359-835X(02)00040-4

35. Spatz H, Kohler L, Niklas K (1999) Mechanical behaviour of plant tissues: composite materials or structures? J Exp Biol 202:3269–3272